Connectivity percolation in suspensions of hard platelets

Maneesh Mathew,[1,*] Tanja Schilling,[2] and Martin Oettel[1,3]

[1]*Institut für Physik, Johannes-Gutenberg-Universität, Staudinger Weg 7, D-55099 Mainz, Germany*
[2]*Theory of Soft Condensed Matter, Université du Luxembourg, 162a avenue de la faïencerie, 1511 Luxembourg, Luxembourg*
[3]*Institut für Theoretische Physik II, Heinrich-Heine-Universität Düsseldorf, Universitätsstr. 1, D-40225 Düsseldorf, Germany*

We present a study on connectivity percolation in suspensions of hard platelets by means of Monte Carlo simulation. We interpret our results using a contact-volume argument based on an effective single-particle cell model. It is commonly assumed that the percolation threshold of anisotropic objects scales as their inverse aspect ratio. While this rule has been shown to hold for rodlike particles, we find that for hard platelike particles the percolation threshold is nonmonotonic in the aspect ratio. It exhibits a shallow minimum at intermediate aspect ratios and then saturates to a constant value. This effect is caused by the isotropic-nematic transition preempting the percolation transition. Hence the common strategy to use highly anisotropic, conductive particles as fillers in composite materials in order to produce conduction at low filler concentration is expected to fail for platelike fillers such as graphene and graphite nanoplatelets.

I. INTRODUCTION

Composite materials of enhanced mechanical strength, thermal conductivity, or electrical conductivity can be produced by mixing polymer resins with nanoparticles. In particular, carbon-based particles such as carbon nanotubes, graphene, and graphite nanoplatelets are promising fillers because of their extraordinary materials properties [1–4]. In this context percolation, a topic that had originally been brought up in the context of fluid flow through porous media, has attained a new field of application.

The term percolation (more specifically connectivity percolation) refers to the transition at which a system changes from containing isolated clusters of particles to containing a system-spanning network that produces connectivity on a macroscopic scale [5,6]. The density at which this transition occurs is called percolation threshold. A composite material made from an insulating matrix that is filled with conductive particles becomes conductive itself when the filler percolates.[1]

For technological applications it is often desirable to use as low a filler content as possible (e.g., because the filler material might be expensive, or it might have a deteriorating influence on other properties of a composite such as its transparency). As it has been argued that the percolation threshold of anisotropic objects should scale as their inverse aspect ratio [7], one commonly uses highly anisotropic fillers such as metal fibers or carbon nanotubes. For rodlike fillers this has been shown to be a successful approach (see, e.g., [8,9]).

Recently, platelike fillers have moved into the focus, in particular due to the development of graphite nanoplatelet reinforced polymer composites [3,4]. While graphite nanoplatelets share some of the promising materials properties of carbon nanotubes, the production of graphite nanoplatelets is in

general less expensive and energy intensive. However, the percolation thresholds that were reached are also not as low as for carbon nanotubes. The authors of a recent review [3] remark that experiments do not show the expected drop of the percolation threshold with increasing aspect ratio.

The topic of percolation in three-dimensional (3D) suspensions of platelets has been addressed in theoretical and numerical investigations [10–16]. However, while much attention has been given to fully penetrable platelets, impenetrable (or otherwise interacting) platelets have, to our knowledge, only been studied in two cases: Ambrosetti and co-workers did a simulation study on percolation in hard, oblate ellipsoids [12], and Otten and van der Schoot addressed the issue briefly in an article on connectedness percolation theory of polydisperse fillers [16]. We will refer to their results in more detail in comparison to our results.

In this paper, we present a Monte Carlo simulation study on connectivity percolation in a suspension of hard platelets in 3D. We discuss, in particular, the dependence of the percolation threshold on the aspect ratio of the platelets, and the interference between the isotropic-nematic transition and the percolation transition. We interpret the simulation data by means of a contact-volume argument based on an effective single-particle cell model.

II. SIMULATION DETAILS

We use hard, cut spheres as model platelets. Real platelets differ from this simple model in many aspects: they vary in shape, are in general not very rigid and often even crumpled, are polydisperse in size, and their interactions are more complex than simple excluded volume interaction (see, e.g., [2,4,17–19]). There are two common features, however: in almost all cases the platelets cannot interpenetrate each other and they have high aspect ratios. Our study is concerned with the effects that these two properties have on the percolation threshold.

A cut sphere is obtained when a sphere of diameter D is intersected with two planes parallel to the equatorial plane at a distance $L/2$ such that the sphere's caps are sliced off [20].

---

*mathewm@uni-mainz.de

[1]In contrast to the case of fluid flow through percolating cavities, however, the filler particles do not need to touch each other. Their distances only need to be small enough to allow for tunneling of a sufficiently large number of charges.

The interaction potential between two platelets is infinite if the platelets overlap and zero otherwise. With this interaction potential the system is purely entropic; its configurational properties do not depend on the temperature T. We use L as the unit of length and $k_B T$ as the unit of energy, where k_B is Boltzmann's constant.

Percolation occurs when the platelets form a system spanning cluster. A cluster is defined as two or more platelets which are connected. We consider two platelets as connected if their surfaces approach closer than a given value A. As we are using periodic boundary conditions, we regard a cluster as percolating if its particles are connected to their own periodic images. In a quantitative comparison to an experiment on electrical conductivity, the distance A would correspond to the tunneling distance. However, the value of A does not have a qualitative effect on the results we present, as long as it is smaller than the particle thickness L.

Monte Carlo simulations were performed for fixed volume V and number of particles N. The volume of one particle is given by

$$V_p = \frac{\pi L}{4}\left(D^2 - \frac{L^2}{3}\right), \tag{1}$$

and the volume fraction is defined by $\eta = N V_p / V$. A cuboid simulation box of dimensions $B \times B \times B$ with periodic boundary conditions was used. Simulations for systems with a connecting distance $A = 0.2L$ involved 1.5×10^6 trial moves per particle for equilibration and 3×10^6 moves per particle for sampling. For the other values of A equilibration and sampling were performed each with 0.5×10^6 moves per particle.

The nematic order parameter S was used to monitor the overall alignment of the platelets [21]. If $\hat{\mathbf{u}}_i$ is a unit vector perpendicular to the surface of platelet i, then S is given by the largest eigenvalue of the tensor

$$\mathbf{Q} = \frac{1}{2N}\sum_i^N (3\hat{\mathbf{u}}_i\hat{\mathbf{u}}_i - \mathbf{I}),$$

where $\mathbf{I}$ is the identity matrix. In a fully aligned configuration S is unity and in a perfectly isotropic configuration it is zero.

III. RESULTS AND DISCUSSION

In an infinite system the percolation transition is marked by a discontinuity; the probability $P(\eta)$ to find a percolating cluster jumps from zero to one at the critical volume fraction η_c^{inf}. In a finite system, the transition is "smeared out"; $P(\eta)$ forms a sigmoidal curve, which becomes steeper with increasing system size (see, e.g., Ref. [5]). In Fig. 1 we show the percolation probability for disks with aspect ratio $D/L = 5$ as a function of volume fraction for several values of the box dimension B. The curves can be fitted by a profile of the form

$$f = \tfrac{1}{2}\{1 + \tanh[a(x - b)]\}, \tag{2}$$

where a is the inverse width of the transition region.

In order to extract η_c^{inf} from the simulation data we employ the finite-size scaling relation [5,22]:
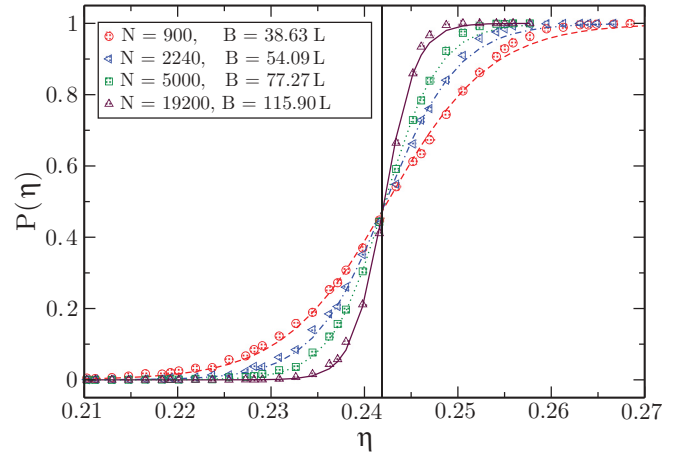
$$a \propto B^{1/\nu}, \tag{3}$$

FIG. 1. (Color online) Percolation probability as a function of volume fraction η for different box sizes B and $D/L = 5$ (N is the number of disks inside the box). The lines are fits by a tanh profile; the solid vertical line marks the infinite system percolation threshold as obtained by a finite-size scaling analysis.

where ν is the correlation length exponent. Figure 2 shows the inverse width a for various system sizes. From the fitted line we find $\nu = 0.96 \pm 0.01$, which is in agreement with the value for percolation in three dimensions (as well as with previous results on spheres and oblate ellipsoids [12,22]).

The volume fractions at the inflection points of the tanh profiles [Eq. (2)] can be interpreted as finite-size percolation thresholds $\eta_c(B)$. Figure 3 shows $\eta_c(B)$ plotted versus $B^{-1/\nu}$. We fitted a line to the data using the value of ν obtained above and extrapolated the fit to $\eta_c^{\text{inf}} = 0.2419 \pm 0.0001$. As the difference between $\eta_c(B)$ and η_c^{inf} is of order 10^{-3}, and as we are interested in the qualitative behavior of the percolation threshold with the aspect ratio, we used the volume fraction at the inflection point as an estimate for η_c^{inf} for all other simulation data presented in the following. (Often, instead of doing a finite-size scaling analysis on the locations of the inflection points, one uses the intersection points of the percolation curves as an estimate for the percolation
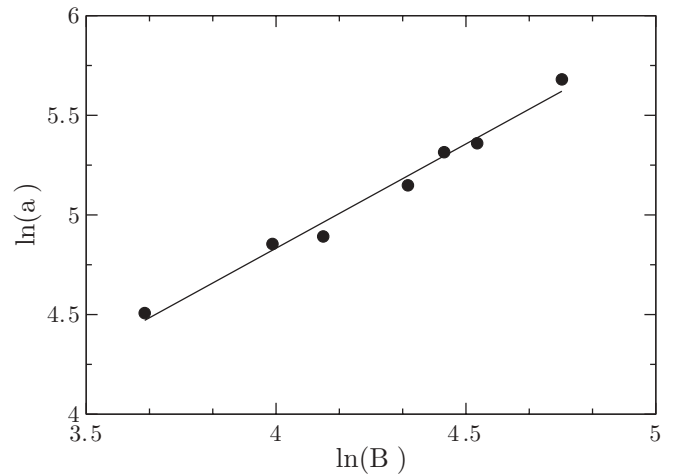

FIG. 2. Inverse transition width a as a function of system size B for $D/L = 5$. The straight line is a fit to the data points. Its slope corresponds to a value of $\nu = 0.96 \pm 0.01$.
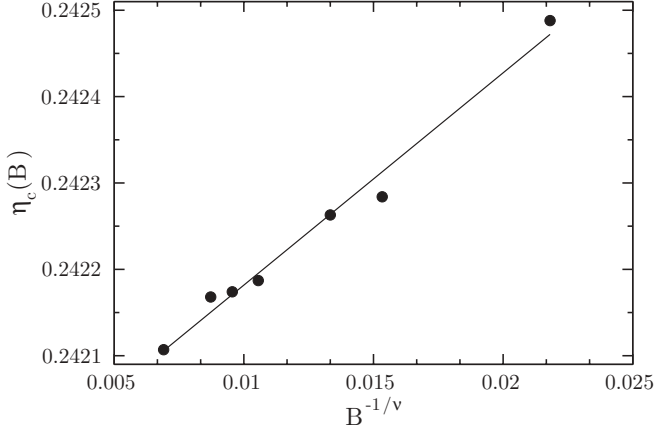
FIG. 3. Percolation threshold as a function of $B^{-1/\nu}$. The line is a fit to the data which yields $\eta_c^{\inf} = 0.2419 \pm 0.0001$.

threshold. In Fig. 1 we marked $\eta_c^{\inf} = 0.2419$ by a vertical line. $\eta_c^{\inf}$ coincides within 10^{-4} with the volume fractions of the intersection region.)

In contrast to the rodlike systems which have been studied in the past, platelets exhibit an interference of the percolation transition with the isotropic-nematic (IN) transition, which leads to nontrivial behavior at the percolation threshold. In Fig. 4, we show the percolation probabilty $P(\eta)$ as a function of the volume fraction η for various aspect ratios D/L (connectivity distance $A/L = 0.2$). The volume fractions at the corresponding IN transitions are marked by dashed lines. For smaller aspect ratios ($D/L \lesssim 8$), percolation occurs at much smaller volume fractions than nematic ordering. For $D/L = 12$ the onset of nematic order and the onset of percolation almost coincide. For larger D/L the situation is reverse: nematic ordering occurs now at much smaller volume fractions than percolation.

Our central result is shown in Fig. 5, which depicts the percolation threshold, η_c, as a function of the aspect ratio D/L for various connectivity distances $A/L = 0.2 \ldots 1$. For
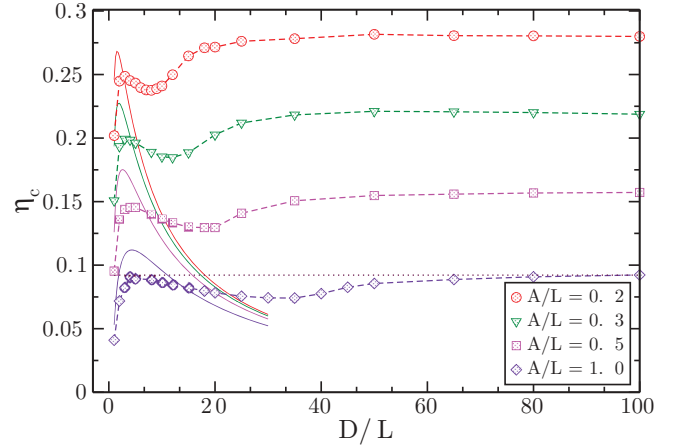
FIG. 5. (Color online) Percolation threshold as a function of disk aspect ratio for various connectivity distances. The solid lines represent the percolation threshold according to the contact volume argument [Eq. (4), $\alpha = 1.7$]. The dotted straight line is the constant value of η_c predicted in Ref. [16] for the case $A/L = 1$.

a given A/L, η_c begins at the known value for hard spheres ($D/L = 1$) [23,24], then quickly rises to a maximum at $D/L \sim 3$ and upon further increasing D/L falls off weakly—until it reaches a minimum at intermediate aspect ratios. Upon further increasing D/L, η_c moderately rises again before finally reaching a plateau value. The effect of increasing the connectivity distance consists in shifting the curves $\eta_c(D/L)$ to lower values and shifting the location of the minimum to higher values of D/L. The occurrence of the mininum and the subsequent plateaulike behavior for higher D/L are consequences of the isotropic-nematic (IN) transition preempting the percolation transition. This can be seen, e.g., when comparing Figs. 4 and 5 for $D/L = 12$ and $A/L = 0.2$. Thus when the behavior of $\eta_c(D/L)$ beyond the minimum is analyzed one should take into account the nematic order in the system. In order to develop an understanding, we discuss the different regimes in detail in turn.

A. Isotropic regime

Based on results for needle-like filler particles one would expect a decrease of η_c with increasing aspect ratio [8,9,25]. This kind of behavior is also predicted by a popular contact-volume argument which, in neglect of specific orientational correlations, assumes that η_c is proportional to the ratio between the hard particle volume V and the overlap volume V_{over} (second virial coefficient) of two hard particles [7]. The proportionality constant α can be loosely associated with the number of next neighbors (contacts) within the overlap volume around one particle [7,25].

For hard disks we have $V(D,L) = V_p$ [Eq. (1)] and $V_{\text{over}}(D,L) = (\pi D^3/3)\{(\cos\theta(1+[\sin^2\theta]/2)+3(\cos\theta + [\theta\sin\theta]/2)(\cos\theta + [\sin^2\theta]/2)\}$ with $\theta = \arccos(L/D)$ [26]. The connectivity criterion set by the minimal distance A between two particles can be incorporated by taking $V_{\text{over}}(D + A, L + A)$ such that

$$\eta_c \approx 2\alpha \frac{V(D,L)}{V_{\text{over}}(D + A, L + A)}. \qquad (4)$$
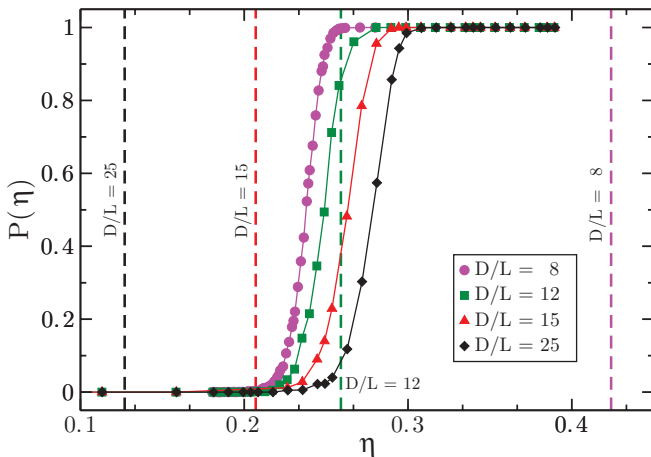
FIG. 4. (Color online) Percolation probability as a function of volume fraction for different aspect ratios ($A = 0.2L$). The symbols and solid lines show the percolation probability; the dashed vertical lines indicate the volume fractions where the nematic order parameter $S = 0.5$ (approximate location of the isotropic-nematic transition).

For $A \lesssim L \ll D$, the contact-volume argument predicts $\eta_c \propto L/D$, i.e., an inverse proportionality with the aspect ratio, similar to the case of rods.

However, such a behavior is completely absent from the data. Our data for the isotropic phase [D/L below the minimum of $\eta_c(D/L)$] are not in a regime in which the asymptotic form of Eq. (4) could be applied (see Fig. 5). Using the full formula for the contact-volume argument (solid lines in Fig. 5), the existence of a maximum near the sphere limit is predicted correctly, however, the subsequent decay with D/L is much too strong. Only for $A = L$ one sees a noticeably weaker D/L dependence. As a result we can state that neglecting orientational correlations leads to a prediction of the behavior of $\eta_c(D/L)$ that is qualitatively wrong.

These findings can be checked against the Ornstein-Zernike approach to the connectedness correlation function. In a study on percolation of hard spheres [24] the so-called "bare chain sum approximation" is introduced which amounts to the following overlap volume criterion:

$$\eta_c \approx \alpha' \frac{V(D,L)}{V_{\text{over}}(D + A, L + A) - V_{\text{over}}(D,L)}. \quad (5)$$

It suffers from an unphysical divergence of η_c when $A \to 0$. For needlelike particles (spherocylinders of length L, radius R, and connectivity distance $2A$ with $L \gg R$) both the contact volume argument (4) and the bare chain sum approximation (5) give the same dependence $\eta_c \propto 1/L$ but the volume quotient in the bare chain sum approximation is larger by a factor $(1 + A/R)/(A/R)$. For disks, however, the bare chain sum approximation ($D \gg L$) gives $\eta_c \propto L/A$ (independent of D) instead of $\eta_c \propto L/D$ from the contact volume argument. This has been found also in Ref. [27] and is consistent with the recent work in Ref. [16] using the Ornstein-Zernike approach in the isotropic fluid. Here in the limit $A \approx L \ll D$ the same D-independent behavior is found: $\eta_{c,\text{OZ}} \approx 2L/[A(5\pi + 6)]$. Indeed for $A = L$ this constant seems to be the correct first-order approximation (see dotted line in Fig. 5) but the other values for A are apparently not compatible with the domain of validity ($A \approx L$) for that result.

The result of a percolation threshold that is independent of aspect ratio is in line with experimental observations [3]. However, as the experimental samples are in general neither homogeneous nor in equilibrium, it is probably not the full explanation of this effect.

B. Nematic regime

For high nematic order ($S > 0.9$) the critical volume fraction $\eta_c(D/L)$ for percolation is in the plateau region (see Fig. 5). For states with high order, one can invoke a single-particle cell model to derive the following expression, which connects volume fraction η, aspect ratio D/L, and order parameter S:

$$\frac{\gamma}{\eta} = 1 + \beta \frac{D}{L} \sqrt{1 - S}. \quad (6)$$

In the cell model, one assumes that each disk occupies an effective volume $V_{\text{eff}} = (\pi/4)D^2 L_{\text{eff}}$ and the effective height of the disk is calculated via the one-particle orientation distribution function (see Appendix), $L_{\text{eff}} = L + \beta D \sqrt{1 - S}$. We determined the constant β as 0.49 by a fit to our data (see Fig. 6), being somewhat smaller than derived from simple guesses for the orientation distribution ($\beta \sim 0.7$). The constant $\gamma = 0.88$ is close to 1, which is consistent with the interpretation that the effective volume for all disks almost fills space. A cell model description is known to be fairly accurate for the columnar phase of disks [28,29], where one can go further and also derive the full partition function. For the percolation problem, we are in the nematic phase but still far away from the columnar phase. Hence it is somewhat surprising that an effective one-particle argument quantifies the value of the order parameter for given volume fraction and aspect ratio also in the nematic phase.

In order to explain the plateau in Fig. 5, we make the assumption that the onset of percolation is dictated by $A \propto L_{\text{eff}} - L$. It is a similar argument as the contact volume argument in the isotropic phase, namely that there is an invariant for percolation which is a quotient between two volumina: the effective excess volume of one disk $(\pi/4)D^2(L_{\text{eff}} - L)$ and the excess overlap volume of two *aligned* disks $\approx (\pi/4)D^2 A$. Using Eq. (6), we immediately find for the critical volume fraction at percolation

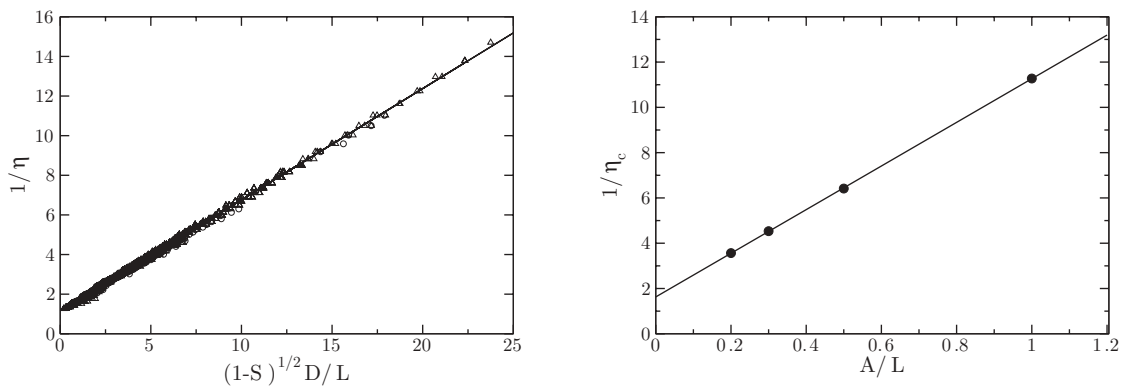$$\frac{\gamma}{\eta_c} = 1 + \beta' \frac{A}{L}. \quad (7)$$

FIG. 6. Left panel: plot of inverse volume fraction $1/\eta$ vs the scaling variable $\sqrt{1 - S}D/L$ for our data deep in the nematic phase with order parameter $S > 0.9$. The linear fit assumes the cell theory equation (6). Right panel: plot of inverse critical volume fraction $1/\eta_c$ at the plateau ($D/L \gg 1$) vs connectivity parameter A/L. The linear fit is according to the volume argument in Eq. (7).
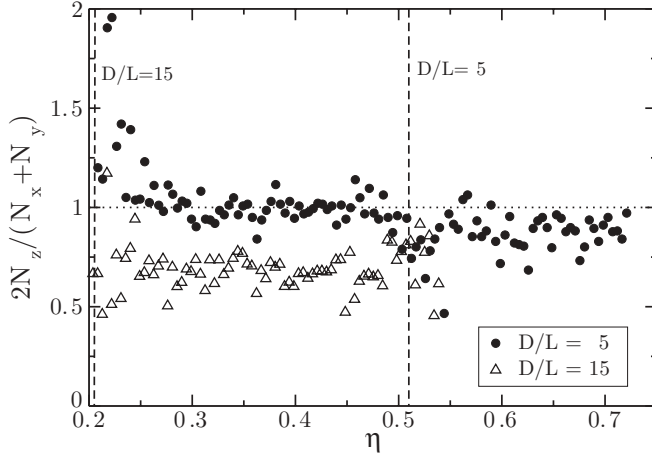
FIG. 7. Ratio of clusters that percolate along the director to clusters that percolate perpendicular to it. The vertical lines mark the IN transition [$S(\eta) = 0.5$].

With this assumption, η_c is indeed independent of D in the nematic phase, as seen in the data. In Fig. 6 we plot the plateau values of $1/\eta_c$ vs A/L and also observe the predicted linear dependence. A linear fit, however, gives $\gamma \approx 0.61$ [in contrast to $\gamma \approx 1$ from the equation of state (6)]. The value of γ is the critical volume fraction for $A = 0$ and thus corresponds to the volume fraction for the jammed state. This simple extrapolation, however, neglects the fact that the system undergoes a transition to the columnar state before reaching such high values for the volume fraction.

When the system is in the isotropic phase, the percolating cluster is connected to its periodic images in all spatial directions with equal probability. As the system undergoes the IN transition an asymmetry develops. In Fig. 7 we show the ratio of clusters that percolate "along the director" (in the z direction) to those that percolate "perpendicular" to the director, i.e., that are connected to their periodic images in the x and/or y direction. Once the system enters nematic phase, percolation along the director becomes less likely.

IV. SUMMARY AND CONCLUSIONS

We have studied connectivity percolation for systems of monodisperse hard platelets modeled by cut spheres of diameter D and height L. The connectivity criterion between two particles was modeled by a minimum surface-to-surface distance A chosen to be of the order of the particle height, $L \sim A$. For a fixed A, we have found that the critical volume fraction η_c for percolation varies surprisingly little with the aspect ratio D/L (see Fig. 5). The most notable feature of $\eta_c(D)$ is a shallow local minimum followed by a plateau for $D/L \gg 1$. We have demonstrated that the appearance of the minimum is directly connected to the onset of nematic ordering in the system. The D-independent, plateaulike behavior of η_c and the variation of the value of η_c on the plateau with A could be rationalized in terms of a contact-volume argument (see Sec. III B). This argument relies on a derivation of the dependence of the nematic order parameter S on aspect ratio D/L and volume fraction η, based on an effective single-particle cell model. We have tested this relation by our simulation results

and found good agreement. In contrast to the nematic phase, a simple interpretation of $\eta_c(D/L)$ in the isotropic phase (small aspect ratios) cannot be given, as angular correlations appear to play a major role. A theoretical approach based on the solution of integral equations for the connectivity correlations appears to be promising in this respect [16]; further work based on fundamental measure density functionals [30,31] and related reference system closures [32,33] is desirable in our opinion.

It is a common strategy to use highly anisotropic, conductive particles as fillers in composite materials to achieve conductivity at low filler concentrations. This strategy is based on a "rule of thumb" which says that η_c decreases with the aspect ratio of anisotropic particles. A major conclusion from our work is that this rule does not hold for platelets such as graphite nanoplatelets. This seems to be in contradiction to the results in Ref. [12] where percolation of hard ellipsoids is studied and the corresponding η_c for oblate ellipsoids (i.e., disks) shows a strong decrease with aspect ratio (see Fig. 3 in Ref. [12]). However, these data are obtained as curves $\eta_c(D/L)$ for constant A/D (and not A/L as in our case), i.e., along these curves the connectivity distance increases with aspect ratio. We have re-analyzed the data in terms of a family of curves for constant A/L and found that apparently all data have been obtained in the isotropic phase and there is little variation of $\eta_c(D/L)$, similar to our findings in the isotropic phase. Hence the authors of Ref. [12] could not see the interference of the IN transition with the percolation transition.

Our study focused on monodisperse hard platelets modeled by cut spheres. In real systems, monodispersity is rather exceptional (for an example using rigid dendrimers, see Ref. [34]). The effects of polydispersity on the percolation threshold in suspensions of anisotropic particles can be subtle—details of the particle size distribution can have large effects as shown in Ref. [16] for the case of rods. If polydispersity does not suppress the IN transition altogether, we expect that the percolation mechanism differs qualitatively between the isotropic and the nematic phase as found here for the monodisperse case. Nevertheless, the detailed behavior of the percolation threshold may depend strongly on the mixture properties and hence one might aim to tailor polydispersity to fine-tune the properties of composite materials.

APPENDIX: CELL MODEL FOR STRONG NEMATIC ORDER

We consider disks deep in the nematic state, i.e., $S \gtrsim 0.9$; see Fig. 8 for geometric definitions for one disk. The deviation of the symmetry axis of one disk (disk orientation) with respect
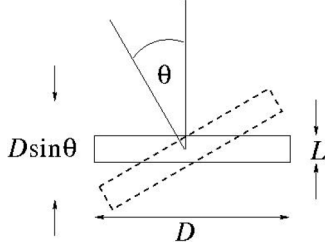
FIG. 8. Geometrical definitions.

to the director is given by θ. The order parameter S is defined by

$$S = \left\langle \frac{3 \cos^2 \theta - 1}{2} \right\rangle, \qquad (A1)$$

where $\langle \ \rangle$ denotes the thermal average. We call $p(\theta)$ the probability distribution function of disk orientations in the bulk state. Using this, the order parameter becomes

$$S = \frac{1}{4\pi} \int d\Omega \, p(\theta) \frac{3 \cos^2 \theta - 1}{2}$$
$$= \frac{1}{2} \int_{-1}^{1} d(\cos\theta) p(\theta) \frac{3 \cos^2 \theta - 1}{2}. \qquad (A2)$$

Through fluctuations around the director, each disk will occupy approximately an effective volume $(D \gg L)$:

$$V_{\text{eff}} = \frac{\pi}{4} D^2 L_{\text{eff}} = \frac{\pi}{4} D^2 \langle L + D \sin\theta \rangle. \qquad (A3)$$

The assumption of our cell model is that the whole system can be considered to be an ensemble of closely packed effective volumes which are occupied by single disks which move independently of each other. In order to determine that effective volume we consider a parametrization of the probability distribution function in the form $p(\theta) = N_\alpha p_{\text{red}}(\theta/\alpha)$, where α is a width parameter in the angular variable and N_α a normalization constant. Furthermore, we consider narrow distributions (large α) which permit us to approximate angular

averages as

$$\frac{1}{2} \int_{-1}^{1} d(\cos\theta) \cdots p(\theta) \approx \int_{0}^{\infty} \theta \, d\theta \cdots p(\theta), \qquad (A4)$$

where the dots stand for any angular variable. Let us define moments of the reduced distribution function by $M_n = \int_0^\infty x^n p_{\text{red}}(x) dx$. Using these definitions, we have the following relations:

$$1 = \int_0^\infty \theta \, d\theta \, p(\theta) = N_\alpha \alpha^2 M_1 \quad \text{(normalization)}, \qquad (A5)$$

$$\frac{L_{\text{eff}} - L}{D} = \int_0^\infty \theta^2 d\theta \, p(\theta) = N_\alpha \alpha^3 M_2 \quad \text{(effective height)}, \qquad (A6)$$

$$1 - S = \frac{3}{2} \int_0^\infty \theta^3 d\theta \, p(\theta) = \frac{3}{2} N_\alpha \alpha^4 M_3 \quad \text{(order parameter)}. \qquad (A7)$$

We can use the equations for normalization and order parameter to eliminate α and N_α and find

$$L_{\text{eff}} = L + D\beta\sqrt{1 - S}\left(\beta = \frac{M_2}{M_1}\sqrt{\frac{2}{3}\frac{M_3}{M_1}}\right), \qquad (A8)$$

where β depends only on the type of reduced distribution p_{red}. As examples, for an exponential distribution $p_{\text{red}}(x) = \exp(-x)$ (as found in the cell theory for the columnar phase [28,29]) we have $\beta = 2/3$ and for a Gaussian distribution $p_{\text{red}}(x) = \exp(-x^2)$ we find $\beta = \sqrt{\pi/6} \approx 0.72$.

As stated before, we proceed with the assumption that the sum of the effective volumes V_{eff} for N particles (almost) fills the system volume V, i.e., $NV_{\text{eff}}/V = \gamma \approx 1$. Using the volume fraction $\eta = N(\pi/4)D^2L/V$ $(D \gg L)$ we rewrite this as $\eta V_{\text{eff}}/[(\pi/4)D^2L] = \gamma$ and upon using Eqs. (A3) and (A8) we find the final result:

$$\gamma = \eta\left(1 + \beta\sqrt{1 - S}\frac{D}{L}\right). \qquad (A9)$$

[1] M. Moniruzzaman and K. I. Winey, Macromolecules **39**, 5194 (2006).

[2] S. Stankovich, D. Dikin, G. Dommett, K. Kohlhaas, E. Zimney, E. Stach, R. Piner, S. Nguyen, and R. Ruoff, Nature (London) **442**, 282 (2006).

[3] B. Li and W. Zhong, J. Math. Sci. **46**, 5595 (2011).

[4] J. Potts, D. Dreyer, C. Bielawski, and R. Ruoff, Polymer **52**, 5 (2011).

[5] D. Stauffer and A. Aharony, *Introduction To Percolation Theory*, 2nd ed. (Taylor & Francis, London, 1994).

[6] R. Meester and R. Roy, *Continuum Percolations* (Cambridge University Press, Cambridge, UK, 1996).

[7] I. Balberg, C. H. Anderson, S. Alexander, and N. Wagner, Phys. Rev. B **30**, 3933 (1984).

[8] H. Deng, R. Zhang, E. Bilotti, J. Loos, and T. Peijs, J. Appl. Polym. Sci. **113**, 742 (2009).

[9] K. Leung and D. Chandler, J. Stat. Phys. **63**, 837 (1991).

[10] E. Charlaix, J. Phys. A: Math. Gen. **19**, L533 (1986).

[11] Y. B. Yi and E. Tawerghi, Phys. Rev. E **79**, 041134 (2009).

[12] G. Ambrosetti, N. Johner, C. Grimaldi, A. Danani, and P. Ryser, Phys. Rev. E **78**, 061126 (2008).

[13] J. A. Quintanilla and R. M. Ziff, Phys. Rev. E **76**, 051115 (2007).

[14] J. Quintanilla, Phys. Rev. E **63**, 061108 (2001).

[15] J. Quintanilla, S. Torquato, and R. Ziff, J. Phys. A: Math. Gen. **33**, L399 (2000).

[16] R. Otten and P. van der Schoot, J. Chem. Phys. **134**, 094902 (2011).

[17] C. Rochette, S. Rosenfeldt, K. Henzler, F. Polzer, M. Ballauff, Q. Tong, S. Mecking, M. Drechsler, T. Narayanan, and L. Harnau, Macromolecules **44**, 4845 (2011).

[18] H. Schniepp, J. Li, M. McAllister, H. Sai, M. Herrera-Alonso, D. Adamson, R. Prud'homme, R. Car, D. Saville, and I. Aksay, J. Phys. Chem. B **110**, 8535 (2006).

[19] L. Harnau, Mol. Phys. **106**, 1975 (2008).

[20] J. A. C. Veerman and D. Frenkel, Phys. Rev. A **45**, 5632 (1992).

[21] P. G. de Gennes and J. Prost, *The Physics of Liquid Crystals* (Oxford University Press, Oxford, 1993).

[22] M. Rintoul and S. Torquato, J. Phy. A: Math. Gen. **30**, L585 (1997).

[23] A. L. R. Bug, S. A. Safran, G. S. Grest, and I. Webman, Phys. Rev. Lett. **55**, 1896 (1985).

[24] T. DeSimone, S. Demoulini, and R. Stratt, J. Chem. Phys. **85**, 391 (1986).

[25] T. Schilling, S. Jungblut, and M. A. Miller, Phys. Rev. Lett. **98**, 108303 (2007).

[26] D. Frenkel, Liq. Cryst. **5**, 929 (1989).

[27] G. Ambrosetti, C. Grimaldi, I. Balberg, T. Maeder, A. Danani, and P. Ryser, Phys. Rev. B **81**, 155434 (2010).

[28] H. H. Wensink, Phys. Rev. Lett. **93**, 157801 (2004).

[29] H. Wensink and H. Lekkerkerker, Mol. Phys. **107**, 2111 (2009).

[30] A. Esztermann, H. Reich, and M. Schmidt, Phys. Rev. E **73**, 011409 (2006).

[31] J. Phillips and M. Schmidt, Phys. Rev. E **81**, 041401 (2010).

[32] M. Oettel, J. Phys.: Condens. Matter **17**, 429 (2005).

[33] A. Ayadim, M. Oettel, and S. Amokrane, J. Phys.: Condens. Matter **21**, 115103 (2009).

[34] L. Harnau, S. Rosenfeldt, and M. Ballauff, J. Chem. Phys. **127**, 014901 (2007).